Solid effect in the electron spin dressed state: A new approach for dynamic nuclear polarization

V. Weis, M. Bennati, M. Rosay, and R. G. Griffin

Citation: The Journal of Chemical Physics **113**, 6795 (2000); doi: 10.1063/1.1310599
View online: http://dx.doi.org/10.1063/1.1310599
View Table of Contents: http://scitation.aip.org/content/aip/journal/jcp/113/16?ver=pdfcov
Published by the AIP Publishing

Solid effect in the electron spin dressed state: A new approach for dynamic nuclear polarization

V. Weis, M. Bennati, M. Rosay, and R. G. Griffin[a)]
MIT/Harvard Center for Magnetic Resonance, Francis Bitter Magnet Laboratory and Department of Chemistry, Massachusetts Institute of Technology, Cambridge, Massachusetts 02139

(Received 3 March 2000; accepted 27 July 2000)

We describe a new type of solid effect for dynamic nuclear polarization (DNP) that is based on simultaneous, near resonant microwave (mw) and radio frequency (rf) irradiation of a coupled electron nuclear spin system. The interaction of the electron spin with the mw field is treated as an electron spin dressed state. In contrast to the customary laboratory frame solid effect, it is possible to obtain nuclear polarization with the dressed state solid effect (DSSE) even in the absence of nonsecular hyperfine coupling. Efficient, selective excitation of dressed state transitions generates nuclear polarization in the nuclear laboratory frame on a time scale of tens of μs, depending on the strength of the electron–nuclear coupling, the mw and rf offset and field strength. The experiment employs both pulsed mw and rf irradiation at a repetition rate comparable to T_{1e}^{-1}, where T_{1e} is the electronic spin lattice relaxation time. The DSSE is demonstrated on a perdeuterated BDPA radical in a protonated matrix of polystyrene. © *2000 American Institute of Physics.* [S0021-9606(00)01340-4]

I. INTRODUCTION

Dynamic nuclear polarization (DNP) is a technique that transfers the substantial Boltzmann polarization of unpaired electron spins to nuclear spins thereby enhancing the nuclear polarization by two or three orders of magnitudes in favorable cases. The sample under investigation must contain a stable or transient paramagnetic species and mw irradiation is applied at or close to the electron Larmor frequency. Depending on the nature of the electron–nuclear interactions, the electron spin polarization is transferred either directly to the nuclei or via an intermediate state in which the electron–electron magnetic dipole couplings play an important role.[1–6] In all cases, however, electron–nuclear coupling—Fermi contact and/or magnetic dipolar coupling—is necessary to drive the transfer of electron spin polarization/coherence into nuclear spin polarization/coherence. Currently, the two primary applications of DNP are the production of polarized targets for nuclear scattering experiments[7] and the enhancement of signal to noise in nuclear magnetic resonance (NMR) experiments.[8–12]

In studies of solids three classes of mechanisms dominate the polarization transfer, *thermal mixing* (TM),[4] the *Overhauser effect* (OE),[5] and the *solid effect* (SE).[1–3] TM is based on a three spin process involving flips of two electrons and one nuclear spin and requires a homogeneous EPR line or an inhomogeneous EPR line at sufficiently high radical concentration to allow electron–electron cross relaxation between individual spin packets.[13] Overhauser DNP takes advantage of selective relaxation pathways due to a time dependent electron–nuclear interaction modulated at the electron Larmor frequency. The standard SE uses the excitation of forbidden electron paramagnetic resonance (EPR) transitions and is described in the electronic laboratory frame. Its efficiency for a given mw excitation field strength is proportional to B_0^{-2}, where B_0 is the laboratory Zeeman field, because it relies on nonsecular hyperfine coupling which does not scale with the Zeeman field. Although all three mechanisms—TM, OE, and the SE—lead, under the correct circumstances, to substantial nuclear polarizations, they do so at a rate that is approximately proportional to T_{1n}^{-1}, where T_{1n} is the nuclear spin lattice relaxation time. (This rate describes the build up of the bulk nuclear magnetization which is a result of an initial fast electron–nuclear polarization transfer step and subsequent nuclear spin diffusion dispersing the polarization throughout the sample. In this paper, however, we only consider the initial electron–nuclear transfer step.) Concurrently, in DNP experiments, it is desirable to have long T_{1n}, typically $\geqslant$30 s, to suppress leakage in the polarization process and thereby to achieve large signal enhancements. This requirement leads in turn to mw irradiation periods of $\geqslant$120 s, and to slow rates of data accumulation. This is a situation reminiscent of that which exists in solid state NMR (SSNMR) of dilute spins—^{13}C, ^{15}N, etc.—where T_{1n} is long and prevents reasonable rates of data acquisition. In the case of SSNMR, the problem is addressed by utilizing polarization transfer from abundant to dilute spins—^{1}H to ^{13}C, ^{15}N, etc.—because the ^{1}H's can be arranged to have a short T_{1n}. At present this transfer can be accomplished in a number of ways, but usually involves some form of Hartmann–Hahn cross polarization.[14] In particular, rf fields satisfying the condition $\omega_{1I}=\omega_{1S}$ are applied to the abundant and dilute spins to accelerate the polarization transfer rate and enhance the polarization.[15]

The experiments described here are a first step toward utilizing similar ideas to perform electron–nuclear polariza-

[a)]Author to whom correspondence should be addressed. Electronic mail: griffin@ccnmr.mit.edu

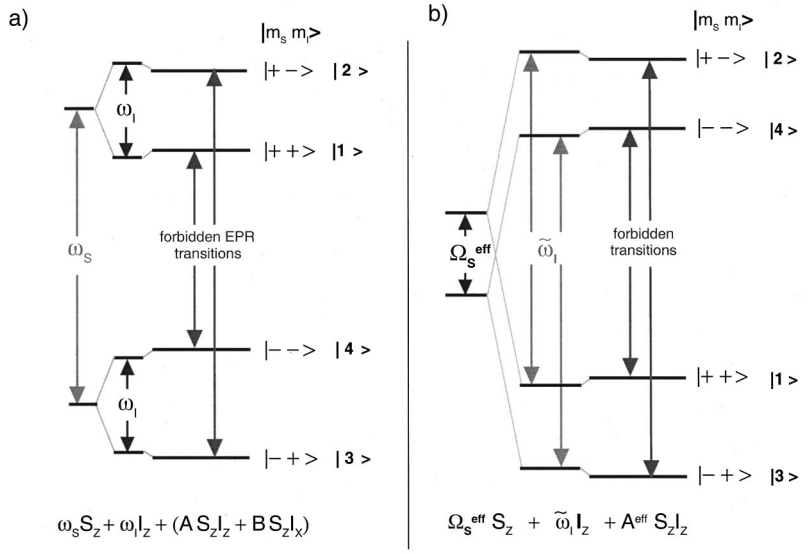

FIG. 1. (a) Four level energy scheme for an electron and a spin 1/2 nucleus in the laboratory frame including the forbidden EPR transitions for the laboratory frame solid effect. The electron Zeeman interaction $\omega_S S_Z$ is the dominant interaction. The anisotropic hyperfine interaction BS_ZI_X is responsible for the nonzero transition probabilities on the forbidden transitions. m_S and m_I are the quantum numbers for the electronic and nuclear Zeeman levels with respect to the Zeeman field. (b) Four level energy scheme for an electron and a spin 1/2 nucleus in the electron spin dressed state. At a Zeeman field of 5 T and with the available mw power, the two EPR transitions at $\Omega_S^{\text{eff}} \pm A^{\text{eff}}/2$ are observable at frequencies close to the electron spin lock field, ω_{1S}. The remaining transitions at $\tilde{\omega}_I \pm A^{\text{eff}}/2$ (NMR) and $\Omega_S^{\text{eff}} \pm \tilde{\omega}_I$ (zero and double quantum) are centered at $\tilde{\omega}_I$ and appear close to the nuclear Larmor frequency ω_I.

tion transfers. In particular, we employ the fact that the electron spin lattice relaxation time, T_{1e}, is several orders of magnitudes shorter than T_{1n} and can be employed to accelerate the polarization transfer process. In addition, we apply mw and rf fields to both the electrons and nuclear spins to perform polarization transfer. Based on this approach we propose a new type of SE in an electron spin dressed state[16–19] for which the presence of nonsecular hyperfine coupling is not required. Instead, the electron–nuclear spin system is subjected to simultaneous mw and rf irradiation. The mw field interacts with the electron spin to create a dressed state[20] in which nuclear magnetic resonance (NMR) transitions, which would be degenerate or forbidden in the absence of the mw field, are selectively excited. Excitation of these transitions transfers electron spin polarization to nuclei in the laboratory frame as is shown in the following sections. The mechanism does not depend explicitly on the Zeeman field and may therefore find application in high field magnetic resonance spectroscopy.

In the following we briefly review the theory of the laboratory frame solid effect, and then present a theoretical description, experimental results, and numerical simulations for the dressed state solid effect (DSSE).

II. THEORY

A. Laboratory frame solid effect (LFSE)

The conventional LFSE is understood with the four level system of an electron and a hyperfine coupled nuclear spin ($I=1/2$) displayed in Fig. 1(a). The laboratory frame Hamiltonian in angular frequencies is

$$H_0=\omega_S S_Z+\omega_I I_Z+AS_ZI_Z+BS_ZI_X, \tag{1}$$

where ω_S and ω_I are the electron and nuclear Larmor frequencies, respectively. A and B represent the secular and nonsecular hyperfine coupling. The eigenvalues of H_0 are given by[21]

$$E_{1/2}=\frac{\omega_S}{2}\pm\frac{1}{2}\left(\omega_I+\frac{A}{2}\right)\cos(\eta_\alpha)\mp\frac{B}{4}\sin(\eta_\alpha),$$

$$E_{3/4}=-\frac{\omega_S}{2}\pm\frac{1}{2}\left(\omega_I-\frac{A}{2}\right)\cos(\eta_\beta)\pm\frac{B}{4}\sin(\eta_\beta), \tag{2a}$$

with

$$\eta_\alpha=\text{atan}\left(\frac{-B}{A+2\omega_I}\right) \quad \text{and} \quad \eta_\beta=\text{atan}\left(\frac{-B}{A-2\omega_I}\right). \tag{2b}$$

The effect of mw irradiation is best analyzed in the electron rotating frame with $H_{\text{mw}}=\omega_{1S}S_X$, where $\omega_{1S}=\gamma_e B_{1S}$ represents the strength of the linearly polarized mw field, B_{1S}. Transformation of H_{mw} into the diagonal frame of H_0 by the unitary transformation U_1 yields[21]

$$\begin{aligned}\tilde{H}_{\text{mw}}&=U_1H_{\text{mw}}U_1^{-1}\\&=\omega_{1S}\cos(\eta)\cdot S_X+\omega_{1S}\sin(\eta)\cdot[S^+I^-+S^-I^+]\\&\quad+\omega_{1S}\sin(\eta)\cdot[S^+I^+ +S^-I^-]\end{aligned} \tag{3a}$$

with

$$\eta=(\eta_\alpha-\eta_\beta)/2$$

and

$$U_1=\exp[-i(\eta_\alpha S^\alpha I_y+\eta_\beta S^\beta I_y)]. \tag{3b}$$

In Eq. (3a) the first term represents the allowed EPR transitions, the second (zero quantum) and third (double quantum)

terms describe the forbidden EPR transitions, and the polarization operators are $S^{\alpha,\beta}=\frac{1}{2}\mathbf{1}\pm S_Z$. In the case of $B=0$ ($\eta=0$), only the single quantum transitions ω_{13},ω_{24} (allowed EPR transitions) are observable in an EPR experiment. The zero and double quantum transitions ω_{23},ω_{14} (forbidden EPR transitions) are not excited because of a vanishing transition dipole moment [$\sin(\eta)=0$]. If the nonsecular hyperfine coupling coefficient B is nonzero, then the forbidden transitions are weakly allowed and four EPR transitions are observed. The probabilities for these transitions are given by[22]

$$\begin{aligned} &P_{\text{allowed}}\propto\cos^2(\eta):\ \Delta m_s=\pm 1,\ \Delta m_I=0,\\ &P_{\text{forbidden}}\propto\sin^2(\eta):\ \Delta m_s=\pm 1,\ \Delta m_I=\pm 1. \end{aligned} \tag{4}$$

When the four level system is at thermal equilibrium [Fig. 1(a)], the selective excitation of one of the forbidden transitions results in the creation of nuclear polarization in both electronic manifolds. The sign of the nuclear polarization is the same for both NMR transitions and depends on which forbidden EPR transition is excited. Selective excitation of only one forbidden transition requires that the excitation bandwidth of the mw irradiation does not concurrently cover both forbidden transitions. From Eqs. (2)–(4) it is obvious that a strong nonsecular hyperfine interaction is required to achieve significant probabilities for the forbidden transitions. However, in a DNP experiment where polarization of the bulk nuclei is the focus, the polarization of strongly hyperfine coupled nuclei is an ancillary effect. These nuclei are ''detuned'' from free bulk nuclei preventing the polarization from dispersing via ^{1}H–^{1}H spin diffusion.[23,24] As a consequence, it is necessary to polarize weakly coupled nuclei, leading to very weak transition probabilities for the solid effect [Eq. (4)]. The predicted B_0^{-2} dependence is in rough agreement with experimental results showing that the LFSE becomes less efficient at higher Zeeman fields. At a field of 5 T ^{1}H-NMR signal enhancements of approximately 10 were obtained at room temperature using a mw power of $\sim$10 W,[9] whereas signal enhancements of $\sim$25 were observed under comparable conditions at 1.4 T and $\sim$13 W of mw power.[25]

B. Dressed state solid effect (DSSE)

Dressed atom states are frequently encountered in optical experiments using strong laser fields for excitation. When a two level system is strongly driven and detected with a weak probe field, a three-peaked spectrum is observed, often referred to as the Mollow spectrum.[16,17] Similarly, a two level electron spin system behaves as a dressed state under strong mw excitation. The DSSE is based on such an electron spin dressed state generated by mw irradiation close to the electron Larmor frequency. The Hamiltonian in the electron rotating frame is given by

$$\begin{aligned} H_{\text{DS}}=H_0+H_{\text{mw}}=&\Omega_S S_Z+\omega_I I_Z+AS_ZI_Z\\ &+BS_ZI_X+\omega_{1S}S_X, \end{aligned} \tag{5}$$

where $\Omega_S=\omega_S-\omega_{\text{mw}}$ is the electron Zeeman frequency offset. The Hamiltonian is transformed into the frame which diagonalizes H_0 and in which H_{mw} is given by Eq. (3). In a second step, we diagonalize the part of the total Hamiltonian which considers allowed EPR transitions, {This is a good approximation for the experiments described here since $\omega_I \gg B$ and η is close to zero for a Zeeman field of 5 T [see Eq. (3)].} i.e., $\tilde{H}_0+\tilde{H}_{\text{mw}}^{\text{allowed}}$. This is achieved by the unitary transformation U_2,[21]

$$U_2=\exp[-i(\theta_\alpha S_Y I^\alpha+\theta_\beta S_Y I^\beta)],$$

$$\theta_\alpha=\operatorname{atan}\left(\frac{-2\omega_{1S}}{A+2\Omega_S}\right)\quad \text{for } A+2\Omega_S\geqslant 0$$

and

$$\theta_\beta=\operatorname{atan}\left(\frac{-2\omega_{1S}}{2\Omega_S-A}\right)\quad \text{for } 2\Omega_S-A\geqslant 0, \tag{6}$$

$$\theta_\alpha=-\pi+\operatorname{atan}\left(\frac{-2\omega_{1S}}{A+2\Omega_S}\right)\quad \text{for } A+2\Omega_S<0,$$

and

$$\theta_\beta=-\pi+\operatorname{atan}\left(\frac{-2\omega_{1S}}{2\Omega_S-A}\right)\quad \text{for } 2\Omega_S-A<0.$$

In this frame the effective Hamiltonian, H^{eff}, is expressed as

$$H^{\text{eff}}=U_2(\tilde{H}_0+\tilde{H}_{\text{mw}}^{\text{allowed}})U_2^{-1}=\Omega_S^{\text{eff}}+\tilde{\omega}_I I_Z+A^{\text{eff}}S_ZI_Z \tag{7}$$

with the eigenvalues

$$E_{1/2}=+\frac{\Omega_S^{\text{eff}}}{2}\pm\left(\frac{\tilde{\omega}_I}{2}+\frac{A^{\text{eff}}}{4}\right), \tag{7a}$$

$$E_{3/4}=-\frac{\Omega_S^{\text{eff}}}{2}\pm\left(\frac{\tilde{\omega}_I}{2}-\frac{A^{\text{eff}}}{4}\right). \tag{7b}$$

In the case $\eta=0$, Ω_S^{eff}, $\tilde{\omega}_I$, and A^{eff} are given by

$$\begin{aligned} &\tilde{\omega}_I=\omega_I,\\ &\Omega_S^{\text{eff}}=\frac{1}{2}\left[\left(\Omega_S+\frac{A}{2}\right)\cos(\theta_\alpha)-\omega_{1S}\sin(\theta_\alpha)\right.\\ &\qquad\left.+\left(\Omega_S-\frac{A}{2}\right)\cos(\theta_\beta)-\omega_{1S}\sin(\theta_\beta)\right], \end{aligned} \tag{8}$$

$$\begin{aligned} A^{\text{eff}}=&\left[\left(\Omega_S+\frac{A}{2}\right)\cos(\theta_\alpha)-\omega_{1S}\sin(\theta_\alpha)\right.\\ &\left.-\left(\Omega_S-\frac{A}{2}\right)\cos(\theta_\beta)+\omega_{1S}\sin(\theta_\beta)\right]. \end{aligned}$$

The corresponding level scheme of the electron spin dressed state is shown in Fig. 1(b). At 5 T ($\omega_I/2\pi=211$ MHz) the nuclear Zeeman interaction $\tilde{\omega}_I$ is the dominant contribution whereas Ω_S^{eff}, A^{eff}, and ω_{1S} are of the order of a few MHz. Therefore, the two EPR transitions (ω_{13},ω_{24}) at $\Omega_S^{\text{eff}}\pm A^{\text{eff}}/2$ are expected to be observable at frequencies close to the mw field strength ω_{1S}. The remaining four transitions at $\tilde{\omega}_I\pm A^{\text{eff}}/2(\omega_{12},\omega_{34})$ and $|\Omega_S^{\text{eff}}\pm\tilde{\omega}_I|(\omega_{14},\omega_{23})$ are centered at $\tilde{\omega}_I$ and therefore at frequencies higher than the EPR transitions.

The level scheme is highly simplified in the case of strong mw irradiation fields $\omega_{1S}\gg|\Omega_S|,|A|$, for which the EPR transitions are determined solely by the mw field

TABLE I. Summary of the transition frequencies and amplitude factors of the dressed state transitions relevant to the generation of nuclear polarization. The results are obtained in the limit of $\Omega_s=0, \omega_{1S} \gg |A|$.

Transition	Transition frequency	Amplitude factor
$\|1\rangle \leftrightarrow \|2\rangle$ $\|3\rangle \leftrightarrow \|4\rangle$	$\left\|\tilde{\omega}_I \pm \frac{A^{\text{eff}}}{2}\right\| = \omega_I$	0
$\|1\rangle \leftrightarrow \|4\rangle$ $\|2\rangle \leftrightarrow \|3\rangle$	$\|\Omega_s^{\text{eff}} \pm \tilde{\omega}_I\| = \|\omega_I \pm \omega_{1S}\|$	$\|\sin(\theta_\alpha)\| = 1$

strength with an effective Zeeman splitting of ω_{1S}. Recently, these transitions were detected experimentally in *X*-band EPR (9 GHz, 0.3 T) using a weak rf probe field with a polarization parallel to the external Zeeman field.[20] Of the four remaining transitions in the electron–nuclear four level system, the NMR transitions are degenerate at ω_I while the zero and double quantum transitions appear at $|\omega_{1S} \pm \omega_I|$ (see Table I).

1. Radio frequency Hamiltonian of the electron dressed state

We now consider the effect of an additional rf irradiation and the possibility of creating nuclear polarization by selective excitation of particular transitions in the electron spin dressed state. The rf irradiation $\omega_{1I}=\gamma_I B_{1X}^I$ is taken as parallel to the nuclear rotating frame *x*-axis given by $H_{\text{rf}} = \omega_{1I} I_X$, where γ_I is the nuclear gyromagnetic ratio. To simplify the analytical expressions, we choose the nonsecular hyperfine constant $B=0$ ($\eta=0$, $U_1=U_1^{-1}=1$). The transformations for $B \neq 0$ are described elsewhere.[21] After transformation into the diagonal frame of H^{eff}, the radio frequency Hamiltonian is

$$\begin{aligned} H_{\text{rf}}^{\text{eff}} = U_2 H_{\text{rf}} U_2^{-1} &= \omega_{1I} \cos(\theta) \cdot I_X + \frac{\omega_{1I}}{2} \sin(\theta) \\ &\quad \cdot \{[S^+ I^- + S^- I^+] - [S^+ I^+ + S^- I^-]\} \\ &= \omega_{1I} \cos(\theta) \cdot \{S^\alpha I_X + S^\beta I_X\} + \frac{\omega_{1I}}{2} \sin(\theta) \\ &\quad \cdot \{[S^+ I^- + S^- I^+] - [S^+ I^+ + S^- I^-]\} \end{aligned} \quad (9)$$

with $\theta=(\theta_\alpha-\theta_\beta)/2$ and $\theta_\alpha, \theta_\beta$ given by Eq. (6).

Clearly, the rf field introduces zero and double quantum terms similar to the mw Hamiltonian in the laboratory frame [Eq. (3)]. However, in contrast to Eq. (3), the angle θ is determined by parameters that can be adjusted in the experiment such as the mw offset Ω_S and the electron spin lock field, ω_{1S} [Eq. (6)]. It is therefore possible to adjust the NMR transition probabilities given by $\cos^2(\theta)$ and $\sin^2(\theta)$ [compare Eq. (4)].

2. Generation of nuclear polarization

In this section we derive an analytical solution for the nuclear laboratory frame polarization assuming on resonant mw irradiation ($\Omega_S=0$) and purely secular hyperfine interaction ($B=0$). We consider only electron spin Boltzmann polarization (S_Z) prior to the experiment so that the density matrix in the laboratory frame is given by $\rho_0=cS_Z$, where c is a constant. The initial electron spin polarization $\langle S_Z \rangle$ is therefore given by $\langle S_Z \rangle = \text{Tr}(S_Z \cdot \rho_0) = c \cdot \text{Tr}(S_Z^2) = c$. In addition, we apply an ideal mw $\pi/2$-pulse with phase *y* to create a state $\rho_1 = c\, S_x$ prior to the evolution under mw and rf. The applied mw spin locking field with phase *x* [Eq. (5)] and strength ω_{1S} creates a low Zeeman field condition for the excited electron spin packets. This condition can also be created by applying a mw pulse sequence consisting of a $\pi/2$-pulse, a short free evolution period and a spin lock pulse of the same phase. During an ideal spin lock pulse the quantization axis and the electron Zeeman splitting are given by the orientation and the strength of the mw field.

The time evolution of ρ_1 under simultaneous mw and rf irradiation is calculated in the diagonal frame of the Hamiltonian H^{eff} [see Eq. (7)] and the nuclear rotating frame according to the following scheme:

$$\rho_1 = cS_X \xrightarrow{U_2 U_1 \rho_1 U_1^{-1} U_2^{-1}} \tilde{\rho}_1 \xrightarrow[\substack{\text{time evolution}\\ \text{under}\\ \text{mw and rf}\\ \text{Hamiltonian}}]{} \tilde{\rho}_2 \xrightarrow{U_1^{-1} U_2^{-1} \tilde{\rho}_2 U_2 U_1} \rho_2$$

$$\rightarrow \langle I_Z \rangle = \text{Tr}(\rho_2 \cdot I_Z).$$

U_1 and U_2 represent the unitary transformations of Eq. (3) and Eq. (6), respectively. Of particular interest is the calculation of laboratory frame nuclear polarization $\langle I_Z(\omega_{1I}, \theta, t_{\text{SL}}) \rangle$ as a function of the spin lock time, t_{SL}, under simultaneous mw and rf irradiation, since it contains information about polarization transfer time and efficiency. The Hamiltonian of interest in the nuclear rotating frame is

$$H = \Omega_S^{\text{eff}} S_Z + \Omega_I I_Z + A^{\text{eff}} S_Z I_Z + H_{\text{rf}}^{\text{eff}} \quad (10)$$

with $\Omega_I = \omega_I - \omega_{\text{rf}}$ being the nuclear Zeeman frequency offset. To understand the effect of the radio frequency irradiation during the evolution of the density matrix $\tilde{\rho}_1$, it is convenient to consider on resonant mw irradiation ($\Omega_S=0$, $\Rightarrow \theta_\beta = -\pi - \theta_\alpha$, $\theta = \pi/2 + \theta_\alpha$) for which the Hamiltonian of Eq. (10) simplifies to

$$H = \Omega_I I_Z + \tfrac{1}{2}[A \cos(\theta_\alpha) - 2\omega_{1S} \sin(\theta_\alpha)] S_Z + H_{\text{rf}}^{\text{eff}}. \quad (11)$$

Although analytical solutions for $\langle I_Z \rangle$ can be derived for the general case, they are not convenient for understanding the spin physics of the experiment. Equations (12a)–(12d) summarize the analytical calculations obtained for $\langle I_Z \rangle$ upon selective excitation of one of the four possible transitions $|i\rangle \leftrightarrow |j\rangle$:

$$|1\rangle \leftrightarrow |4\rangle: \tilde{\rho}_1 \rightarrow \langle I_Z \rangle = + \frac{c}{2} \sin(\theta_\alpha) \times \{1 - \cos[\omega_{1I} t_{\text{SL}} \cos(\theta_\alpha)]\}, \quad (12a)$$

$$|2\rangle \leftrightarrow |3\rangle: \tilde{\rho}_1 \rightarrow \langle I_Z \rangle = - \frac{c}{2} \sin(\theta_\alpha) \times \{1 - \cos[\omega_{1I} t_{\text{SL}} \cos(\theta_\alpha)]\}, \quad (12b)$$

$$|1\rangle \leftrightarrow |2\rangle: \tilde{\rho}_1 \rightarrow \langle I_Z \rangle = 0, \quad (12c)$$

$$|3\rangle \leftrightarrow |4\rangle : \tilde{\rho}_1 \rightarrow \langle I_Z \rangle = 0. \tag{12d}$$

It can be seen that nuclear polarization is generated if one of the pathways in Eqs. (12a) and (12b) is selectively excited. Selective excitation is practically always possible since the rf excitation bandwidth is smaller than the spectral separation of the zero and double quantum transitions given by $|\omega_{14} - \omega_{23}| = 2\Omega_S^{\text{eff}} = 2\sqrt{(A/2)^2 + \omega_{1S}^2}$. The sign of the polarization depends on the transition selected. Both pathways display an oscillatory behavior in t_{SL} with a frequency $\omega_{1I}\cos(\theta_\alpha)$. In comparison, a fully allowed NMR transition would exhibit a nutation frequency of ω_{1I}. Therefore, the results of Eq. (12) can be interpreted in terms of allowed and forbidden NMR transitions in a manner similar to the EPR transitions used in the LFSE [Eq. (4)]. It is this analogy that leads to the term dressed state solid effect (DSSE).

The results indicate the importance of the mw irradiation field strength, ω_{1S}. If ω_{1S} is reduced, the angle θ_α decreases and reduces the amplitude factors in Eqs. (12). In the limit of $\omega_{1S} \rightarrow 0$, no nuclear polarization is generated for any value of t_{SL}.

Clearly, maximum electron spin polarization is transferred to the nuclei for rf pulse durations of $t_{\text{SL}} = \pi/(\omega_{1I}\cos(\theta_\alpha))$. Unfortunately, the build-up time for the polarization approaches infinity if the amplitude factor is maximized. For realistic DNP applications, however, the polarization must be accumulated within the electronic relaxation time during spin lock $T_{1\rho}$ which is typically 10–100 μs. A faster polarization transfer rate can only be achieved by a reduction in the amplitude of the maximum value for $\langle I_Z \rangle$.

To illustrate this idea we discuss the situation encountered in the experimental section. mw is irradiated on resonance ($\Omega_S = 0$) with a field strength ω_{1S} larger than the hyperfine couplings of the nuclei ($\omega_{1S} \gg A$). For this case, the values for the transition frequencies and the amplitude factors are given in Table I. As mentioned previously, two dressed state transitions are degenerate at the free nuclear Larmor frequency ω_I. This is due to the effect of the strong mw irradiation which decouples the hyperfine interaction to the nuclei ($A^{\text{eff}} = 0$). These transitions are not useful for a DNP experiment since their amplitude factors vanish under the given conditions and do not allow for the build up of nuclear polarization. The remaining two transitions (zero and double quantum) are symmetrically positioned around ω_I with a distance corresponding to the mw field strength ω_{1S}. Using Eqs. (12a) and (12b) it can be shown that the transfer of the entire electron spin polarization would require an infinite time t_{SL} and is therefore not practicable. However, for typical proton rf field strengths ($\omega_{1I}/2\pi \sim 100$ kHz), transfer times of 10 μs allow a transfer of up to ~85% of the initial electron spin polarization depending on the ratio of ω_{1S} and A.

Finally we want to emphasize that the above expressions are derived under the assumption of purely secular hyperfine coupling, which is a reasonable approximation for the hyperfine interaction in solid samples at high Zeeman fields. In the case of a liquid with short correlation times, the isotropic hyperfine interaction represents the exact description at any Zeeman field. This suggests that the DSSE should be observable in liquid solution.

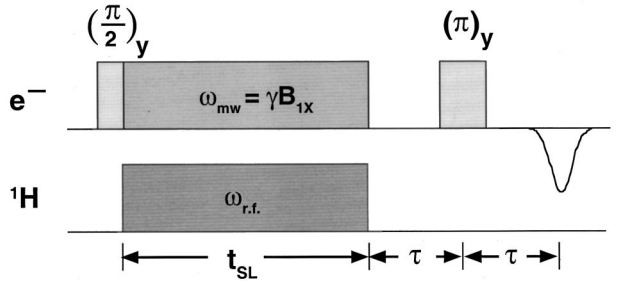

FIG. 2. Pulse sequence for the dressed state solid effect (DSSE). The electron spin echo intensity is monitored after an electron spin lock sequence of duration t_{SL} and a refocusing π-pulse at a time τ after the spin lock pulse. The echo intensities of two sequences with and without rf pulse during the electron spin lock are subtracted and recorded as a function of the rf frequency, ω_{rf}.

III. EXPERIMENT

The experiments were performed with a custom design pulsed EPR spectrometer operating at 139.5 GHz/5 T. An IMPATT diode network (Donetsk Physico Technical Institute) permits mw power amplification and fast amplitude modulation (<10 ns rise and fall times) as well as phase switching (0°, 90°, 180°, 270°) of the 36–38 mW output power.[26] mw $\pi/2$-pulses are ~120 ns using a helical multiple frequency resonator.[27] The rf (NMR) circuit consists of a parallel LC circuit with a series matching capacitor. During the rf sweep tuning and matching is maintained with a computer controlled stepping motor recently developed for ENDOR experiments.[26]

DSSE experiments were performed on a powder sample of perdeuterated bis-diphenylene-phenyl-allyl (BDPA) dispersed at a level of ~1% by weight in a protonated polystyrene matrix. Deuteration of the BDPA molecule insures that no strong hyperfine couplings are present. The samples were evacuated on a high vacuum line to remove oxygen in order to lengthen T_{1e}. For 0.7 mm o.d. sample tubes, the volume in the active cavity amounts to 0.3 μl. Because of the small sample the ^{1}H signal was detected indirectly by monitoring the attenuation of the electron spin echo intensity. All experiments were performed at room temperature.

Figure 2 displays the pulse sequence to detect the DSSE. The electron spin echo intensity was monitored after an electron spin lock of duration t_{SL} and a refocusing π-pulse at a time τ after the spin lock. The echo intensities observed in the two sequences with and without the rf pulse during the electron spin lock were subtracted to yield the positive absorption line shape in Fig. 4. The echoes were recorded as a function of the rf frequency, and at each setting 200 transients were averaged.

IV. RESULTS AND DISCUSSION

A. EPR and ENDOR

The 139.5 GHz EPR spectrum (not shown) of the BDPA-d_{21} consists of a nearly axially symmetric g-tensor

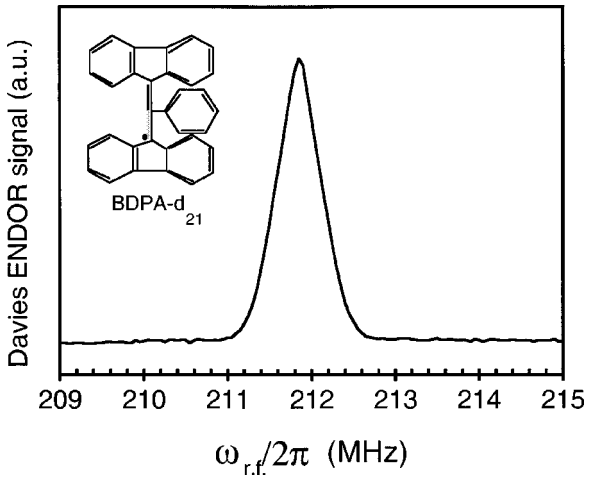

FIG. 3. ^{1}H Davies ENDOR spectrum of perdeuterated bis-diphenylene-phenyl-allyl (BDPA) in a protonated polystyrene matrix at 5 T ($\omega_I/2\pi = 211.8$ MHz). The structure of the BDPA radical is shown in the inset. The pulse lengths were 280 ns for a mw π pulse and 4.5 μs for the ^{1}H rf pulse.

with a span of 6.5 G. The corresponding proton DAVIES ENDOR spectrum is shown in Fig. 3 and displays a single line at the free proton Larmor frequency (211.85 MHz), indicating that no hyperfine couplings of more than 1.2 MHz are present. The strong intensity of the matrix peak (at the free proton Larmor frequency) is due to the large number of distant protons.[28]

B. Dressed state solid effect

Experimental results obtained with the pulse sequence of Fig. 2 are shown in Fig. 4 for various settings of the mw and rf field strengths, respectively. The Zeeman field was set to be on resonance with the maximum of the EPR line. The electron spin lock time, t_{SL}, was constant during the experiments at 3 μs. For large mw field strengths, the typical three peaked dressed state spectra are observed. They consist of two peaks symmetrically about the ^{1}H free larmor frequency and an additional peak at $\omega_I = 211.85$ MHz. The positions of the satellites are mw power dependent and shift towards ω_I when the mw B_{1S}-field is reduced (full mw power, $\omega_{1S}/2\pi = \pm 1.75$ MHz; -6 dB, $\omega_{1S}/2\pi = \pm 0.91$ MHz; -12 dB, $\omega_{1S}/2\pi = \pm 0.51$ MHz). In fact, their shift is almost linear in B_{1S}, which can be understood in the DSSE model. In the case $\Omega_S = 0, \omega_{1S} \gg |A|$ the zero and double quantum transitions are located at $\omega_I \pm \omega_{1S}$. Thus, reducing the mw field strength ω_{1S} results in a linear shift of these transitions towards ω_I. The fact that the observed shift is not perfectly linear is attributed to the relatively weak spin lock field which does not fulfill the condition $\omega_{1S} \gg |A|$. In addition to the line shift, the width of the satellite peaks is clearly reduced by reducing the B_{1S}-field. A reduction of the rf power only results in an overall signal decrease without additional effects. Experimental results are shown in Fig. 4 for three rf power settings of 350, 120, and 50 W ($\omega_{1H}/2\pi \sim 100$ kHz at 350 W).

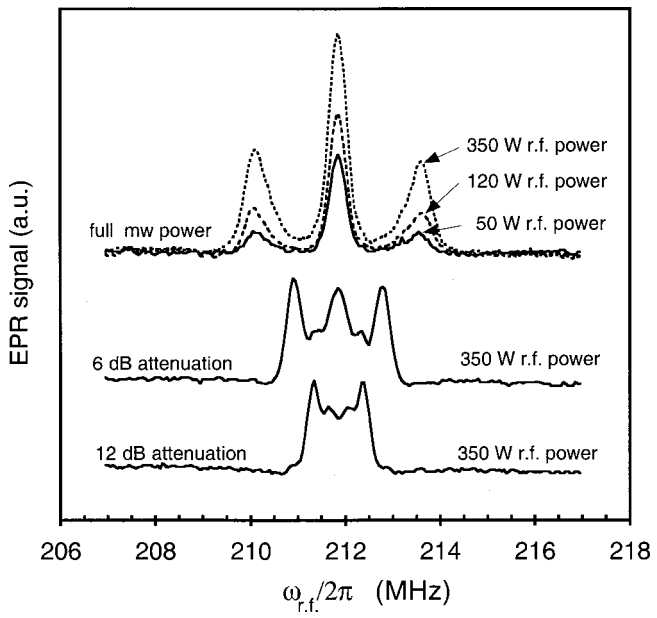

FIG. 4. DSSE experiment on perdeuterated BDPA for various settings of the mw spin lock field (0 dB, 6 dB, and 12 dB attenuation) and the rf power level (350 W, 120 W, and 50 W) for a spin lock time $t_{SL} = 3$ μs. The mw $\pi/2$ pulse length was 140 ns and the ^{1}H field during electron spin lock $\sim$100 kHz at 350 W.

In addition to the satellite peaks, a signal is observed at the free ^{1}H Larmor frequency which corresponds to the degenerate $|1\rangle$–$|2\rangle$ and $|3\rangle$–$|4\rangle$ transitions in the limit $\Omega_S = 0, \omega_{1S} \gg |A|$. This peak intensity shows a pronounced dependence on the mw B_{1S}-field strength which is not observed for the satellite transitions, indicating that the central peaks are driven more efficiently by the applied rf irradiation due to a larger transition dipole moment as compared to the satellite peaks. Indeed, this is consistent with the effective rf Hamiltonian H_{rf}^{eff} of Eq. (9) in the limit $\Omega_S = 0, \omega_{1S} > |A|$. For $|\theta_\alpha| < \pi/4$ $(2\omega_{1S} < A)$ the $|1\rangle$–$|4\rangle$ and $|2\rangle$–$|3\rangle$ transitions have higher transition probabilities than the $|1\rangle$–$|2\rangle$ and $|3\rangle$–$|4\rangle$. In contrast, for $2\omega_{1S} > A$, the zero and double quantum transitions are driven less efficiently which is the situation for the perdeuterated sample. In addition, this behavior was confirmed in numerical simulations discussed in the next section. It should be mentioned that two other mechanisms can give rise to a signal contribution at ω_I. First, an ENDOR matrix peak of weakly coupled protons can occur, although the pulse sequence is not typical of ENDOR experiments. It is well known that ENDOR effects are observable for mw and rf pulses which deviate significantly from the ideal π-pulses used in the Davies Endor sequence. Second, it was recently stated[21] that a nonideal mw pulse can generate nuclear coherence even without rf irradiation. This is, however, only possible in the presence of nonsecular hyperfine coupling, $B \neq 0$. In this case, the rf pulse during electron spin lock might transform the nuclear coherence into nuclear polarization thereby affecting the EPR polarization.

C. DSSE simulations

Numerical simulations of the DSSE experiment were performed with the complete Hamiltonian ($B = 0$) using the GAMMA (Ref. 29) simulation platform. In addition to the experimental data, we calculated both the EPR signal $\langle S_X \rangle$ as

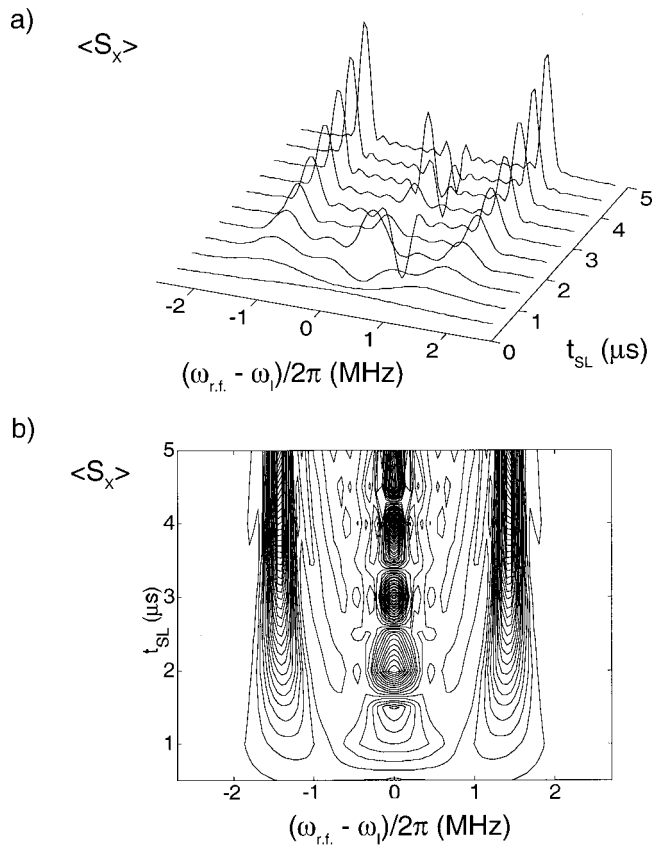

FIG. 5. (a) Calculated time evolution of the electron spin lock magnetization $\langle S_X \rangle$ as a function of the radio frequency $\omega_{rf}/2\pi$ and its contour plot (b). The simulation was performed as described in the text with the following parameters: $\omega_{1S}/2\pi = 1.4$ MHz, $\omega_{1I}/2\pi = 85$ kHz, $A = 0.5$ MHz.

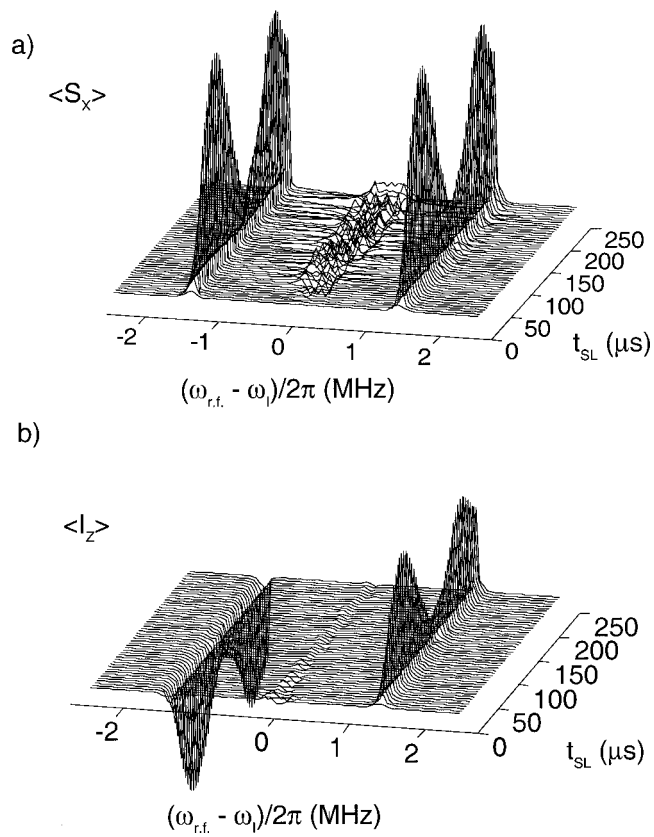

FIG. 6. (a) Calculated time evolution of the electron spin lock magnetization $\langle S_X \rangle$, and the nuclear polarization $\langle I_Z \rangle$ (b) as a function of the radio frequency $\omega_{rf}/2\pi$ over an extended time period $t_{SL} = 0-250$ μs. The simulation was performed with the following parameters: $\omega_{1S}/2\pi = 1.4$ MHz, $\omega_{1I}/2\pi = 85$ kHz, $A = 0.2$ MHz.

well as the NMR signal $\langle I_Z \rangle$. The simulations were performed by calculating datasets with and without rf irradiation and subsequently subtracting the two datasets. The density matrix prior to the pulse sequence contained only electron spin polarization S_Z. An isotropic g-factor as well as isotropic hyperfine coupling are assumed and electron offset effects were taken into account by integrating over a Gaussian EPR line shape. In order to reduce computational time, the signals were determined with the density matrix immediately after the spin lock pulse. The additional free evolution and the refocusing π-pulse used in the experiment do not need to be considered in the simulation since their purpose is only the creation of a detectable EPR signal. Figure 5 displays a calculated signal $\langle S_X \rangle$ for on resonant mw irradiation ($\Omega_S = 0$), $\omega_{1S}/2\pi = 1.4$ MHz, an isotropic hyperfine coupling of $A = 0.5$ MHz, and a series of spin lock times up to 5 μs. It can be seen that the signal close to ω_I undergoes several oscillations with an intensity comparable to the satellite peaks whose intensity increases monotonically. From the contour plot [Fig. 5(b)] the fast nutation behavior of the central line is more apparent.

As predicted in the Theory, excitation of either satellite transition allows for build up of nuclear polarization with opposite sign as demonstrated in Fig. 6 which displays the time evolution of both $\langle S_X \rangle$ and $\langle I_Z \rangle$ for an extended period of time (0–250 μs) assuming a hyperfine coupling $A = 0.2$ MHz. The plot shows that the detection of $\langle S_X \rangle$ is an indirect measure of the nuclear polarization as long as the satellite peaks are considered. Both signals reach their maximum values for a spin lock time of ~ 75 μs which is consistent with the time $t_{SL} = \pi/[\omega_{1I} \cos(\theta\alpha)]$ derived in the theory section. With $\omega_{1I}/2\pi = 85$ kHz, $\omega_{1S}/2\pi = 1.4$ MHz, and $A = 0.2$ MHz we find a value of $t_\pi = 82$ μs.

The central transition in the $\langle S_X \rangle$ signal does not allow for a significant generation of $\langle I_Z \rangle$ with the parameters chosen in the simulation. This observation is consistent with the predictions displayed in Table I, which indicate that excitation of the degenerate transitions at ω_I does not generate nuclear polarization at any spin lock duration.

The central peak in the $\langle S_X \rangle$ signal deserves a closer look. Although it is always present in the experiment and even exceeds the DNP transitions in several cases, it is not predicted by the theory and not found in the simulations. We attribute this experimental fact to a strong residual ENDOR matrix peak involving many weakly hyperfine coupled protons as detected in the Davies ENDOR experiment (see Fig. 3). It was recently shown that a simulation of the matrix peak needs to take into account a large number of weakly coupled nuclear.[28] The simulations presented in this section, however, were performed on an electron–nuclear two spin system. It is therefore not surprising that the matrix peak is not reproduced in the simulation of the DSSE experiment.

The experiments and calculations demonstrate that

nuclear polarization is created by excitation of electron spin dressed state transitions, and results in a build-up of polarization of opposite sign upon excitation of either satellite transition. In this respect the experiment is an analogue of the DNP solid effect in the laboratory frame.

V. CONCLUSIONS

We have shown that the solid state effect in the electron spin dressed state can be used to create nuclear polarization based on experiments in which the loss of electron spin polarization was detected. Although the experiment does not directly detect nuclear polarization, we are convinced that it is generated for several reasons. First, indirect detection of polarization transfer has been successfully applied in both nuclear–nuclear[14] and electron–nuclear[30] polarization transfer schemes. Second, the experimental results are fully supported by simulations which include the evolution of the full density matrix. These simulations unambiguously correlate the observed spectra with the generation of nuclear polarization. Third, any residual ENDOR effect can be ruled out because the DSSE transitions appear at positions well outside the spectral region of any detected hyperfine coupling.

The available time for the polarization transfer is determined by the electronic relaxation time $T_{1\rho}$ during spin lock. This time does not impose severe restrictions since the probabilities for the DNP transitions are significantly higher than in the electron lab frame version of the experiment. In addition, one can repeat the polarization sequence with a rate in the order of $1/T_{1e}$ to accumulate nuclear polarization.

Our results anticipate that the DSSE has a significant advantage over the LFSE experiment which arises from hyperfine decoupling during near resonance mw irradiation. Nuclei with hyperfine couplings A, $B < \omega_{1S}$ are experiencing a reduced effective coupling due to mw irradiation. In the limit of A, $B \ll \omega_{1S}$ the nuclei are entirely decoupled, resulting in NMR frequencies ω_I independent of the hyperfine coupling terms A and B. As a result, we expect the polarized protons to undergo efficient proton–proton spin diffusion with the bulk protons since the nuclear dipole–dipole couplings remain unaffected by the mw irradiation.

Finally, the DSSE—in contrast to the LFSE experiment—does not rely on nonsecular hyperfine coupling $BS_Z I_X$. Instead, the off diagonal elements of the Hamiltonian are introduced by the mw field. Therefore, the experiment should function in liquids where the anisotropic part of the hyperfine interaction is averaged to zero by pseudo-isotropic molecular motion.

To date, the DNP effect was detected indirectly by monitoring the attenuation of the spin locked electron magnetization. Since the experiment requires a highly efficient probe for simultaneous mw and rf irradiation, it currently can be performed only in our 140 GHz pulsed EPR/ENDOR setup using a mw resonance structure and very small sample. Work is in progress to increase the sensitivity of the NMR detection to provide a direct measure of the nuclear polarization $\langle I_Z \rangle$.

ACKNOWLEDGMENT

This research was supported by the National Institutes of Health GM-35382 and RR-00995.

[1] A. Abragam and W. G. Procter, C. R. Acad. Sci. URSS **246**, 2253 (1958).
[2] E. Erb, J. L. Motchane, and J. Uebersfeld, C. R. Acad. Sci. URSS **246**, 2121 (1958).
[3] C. D. Jeffries, Phys. Rev. **106**, 164 (1957).
[4] B. N. Provotorov, Sov. Phys. JETP **14**, 1126 (1962).
[5] A. W. Overhauser, Phys. Rev. **92**, 411 (1953).
[6] A. Abragam and M. Goldman, *Nuclear Magnetism: Order and Disorder* (Clarendon, Oxford, 1982).
[7] W. de Boer, J. Low Temp. Phys. **22**, 185 (1976).
[8] R. A. Wind, M. J. Duijvestijn, C. v. d. Lugt, A. Manenschijn, and J. Vriend, Prog. Nucl. Magn. Reson. Spectrosc. **17**, 33 (1985).
[9] L. R. Becerra, G. J. Gerfen, R. J. Temkin, D. J. Singel, and R. G. Griffin, Phys. Rev. Lett. **71**, 3561 (1993).
[10] M. Afeworki, S. Vega, and J. Schaefer, Macromolecules **25**, 4100 (1992).
[11] D. A. Hall, D. A. Maus, G. J. Gerfen, S. J. Inati, L. R. Beccera, F. W. Dahlquist, and R. G. Griffin, Science **276**, 930 (1997).
[12] G. J. Gerfen, L. R. Becerra, D. A. Hall, D. J. Singel, and R. G. Griffin, J. Chem. Phys. **102**, 9494 (1995).
[13] D. A. Hall, C. T. Farrar, G. J. Gerfen, S. J. Inati, and R. G. Griffin, J. Chem. Phys. (submitted).
[14] S. R. Hartmann and E. L. Hahn, Phys. Rev. **128**, 2042 (1962).
[15] A. Pines, M. S. Gibby, and J. S. Waugh, J. Chem. Phys. **59**, 569 (1973).
[16] B. R. Mollow, Phys. Rev. **188**, 1969 (1969).
[17] F. Y. Wu, S. Ezekiel, M. Ducloy, and B. R. Mollow, Phys. Rev. Lett. **38**, 1077 (1977).
[18] C. Cohen-Tannoudji, J. Dupont-Roc, and G. Grynberg, *Atom–Photon Interactions: Basic Processes and Applications* (Wiley, New York, 1992).
[19] C. Wei, S. A. Holmstrom, A. D. Greentree, and N. B. Manson, J. Opt. B: Quantum Semiclassical Opt. **1**, 289 (1999).
[20] G. Jeschke, Chem. Phys. Lett. **301**, 524 (1999).
[21] G. Jeschke and A. Schweiger, Mol. Phys. **88**, 355 (1996).
[22] W. B. Mims, Phys. Rev. B **5**, 2409 (1972).
[23] A. D. A. Hansen and J. P. Wolfe, Phys. Lett. **66A**, 320 (1978).
[24] P. F. A. Verheij, W. T. Wenckebach, and J. Schmidt, Appl. Magn. Reson. **5**, 187 (1993).
[25] M. J. Duijvestijn, R. A. Wind, and J. Smidt, Physica (Utrecht) **138B**, 147 (1986).
[26] M. Bennati, C. Farrar, J. Bryant, S. Inati, V. Weis, P. Riggs-Gelasco, J. Stubbe, and R. G. Griffin, J. Magn. Reson. **138**, 232 (1999).
[27] V. Weis, M. Bennati, M. Rosay, J. A. Bryant, and R. G. Griffin, J. Magn. Reson. **140**, 293 (1999).
[28] A. V. Astashkin and A. Kawamori, J. Magn. Reson. **135**, 406 (1998).
[29] S. A. Smith, T. O. Levante, B. H. Meier, and R. R. Ernst, J. Magn. Reson., Ser. A **106**, 75 (1994).
[30] D. J. van den Heuvel, A. Henstra, T. S. Lin, J. Schmidt, and W. T. Wenckebach, Chem. Phys. Lett. **188**, 194 (1991).